catalysts

MDPI

Article

Highly Reducible Nanostructured CeO_2 for CO Oxidation

Gang Feng, Weining Han, Zhimiao Wang, Fang Li and Wei Xue *

Hebei Provincial Key Laboratory of Green Chemical Technology and High Efficient Energy Saving, School of Chemical Engineering and Technology, Hebei University of Technology, Tianjin 300130, China; greenchem309@gmail.com (G.F.); zhaoqingqing1985@gmail.com (W.H.); wzmcat309@gmail.com (Z.W.); lifang@hebut.edu.cn (F.L.)

* Correspondence: weixue@hebut.edu.cn; Tel.: +86-22-6020-2419

Received: 30 September 2018; Accepted: 5 November 2018; Published: 11 November 2018

Abstract: Ceria in nanoscale with different morphologies, rod, tube and cube, were prepared through a hydrothermal process. The structure, morphology and textural properties were characterized by X-ray diffraction (XRD), scanning electron microscope (SEM), transmission electron microscope (TEM) and isothermal N_2 adsorption-desorption. Ceria with different morphologies were evaluated as catalysts for CO oxidation. CeO_2 nanorods showed superior activity to the others. When space velocity was 12,000 mL·gcat^{-1}·h^{-1}, the reaction temperature for 90% CO conversion (T_{90}) was 228 °C. The main reason for the high activity was the existence of large amounts of easily reducible oxygen species, with a reduction temperature of 217 °C on the surface of CeO_2 nanorods. Another cause was their relatively large surface area.

Keywords: ceria; morphology; catalyst; CO oxidation; surface oxygen species

1. Introduction

Ceria (CeO_2) is a significant rare earth oxide and has widespread applications. It can be used in the fields of luminescent materials [1], gas sensors [2], electronic ceramics [3], biology, medical science [4,5] and so on. In the field of catalysis, CeO_2 can be used as catalysts or non-inert support for heterogeneous catalysts [6–8], acting as an oxygen buffer through a fast Ce^{3+}/Ce^{4+} cycle involving the participation of lattice oxygen. Therefore, it has been extensively studied and applied in many fields, such as three-way catalysts [9,10], fuel cells [11], water–gas shifts [12], ethanol dehydrogenation [13], CO oxidation [14], alcohol steam reforming [15] and photocatalysis [16]. Usually, the catalytic reactivity of CeO_2 not only depends on the particle size but is also closely related to its morphology [17]. Yuan et al. [18] prepared a Pd-based catalyst using CeO_2 nanotubes as support for oxidative carbonylation of phenol to diphenyl carbonate (DPC) and obtained higher activity and DPC selectivity than those of Pd catalyst supported on the zero-dimensional CeO_2 particles. Gawade et al. [19] studied the water gas shift reactions catalyzed by Cu/CeO_2 and found that the CeO_2 nanoparticle supported catalyst achieved much higher CO conversion than a catalyst supported on CeO_2 nanorods. The results can be explained by the highly dispersed copper species over CeO_2 nanoparticles that constitute the active sites for the water gas shift reaction.

CO catalytic oxidation is an effective pollutant removal technology and is also a typical probe reaction that is widely used for studying the catalyst structure, adsorption/desorption and the reaction mechanism [20]. There are two groups of catalysts for CO oxidation: non-noble metal catalysts and supported noble metal catalysts [21]. CeO_2 is one of the CO oxidation catalysts that have attracted much attention in recent years [20]. Both size and morphology of CeO_2 particles has a significant impact on their catalytic performance in CO oxidation. Tana et al. [22] studied the morphology-dependent

phenomenon of CeO_2 for CO oxidation. It was found that CeO_2 nanowires and nanorods, which mainly showed the reactive {110} and {100} planes, resulted in much higher activity for CO oxidation than CeO_2 particles. The CeO_2 nanowires that exposed more active planes exhibited the highest activity. González-Rovira et al. [23] prepared CeO_2 nanomaterials with a tubular structure by an electrochemical method. The outer diameter of the nanotubes was about 200 nm with lengths between 30 and 40 μm. The activity of the CeO_2 nanotubes was 400 times higher than CeO_2 particles for CO oxidation under certain conditions. Zhang et al. [24] synthesized cauliflower like CeO_2 through the decomposition of Ce-BTC (BTC: 1,3,5-benzenetricarboxylic acid) straw and found that it exhibited excellent catalytic activity and stability in CO oxidation. The superior catalytic performance could be ascribed to the cauliflower like structure, which was composed of porous CeO_2 nanorods that provided more active sites and oxygen vacancy for CO oxidation. Nowadays many papers have been published with the title 'CO oxidation on CeO_2 with different morphologies' [20]. However, different researchers usually got different activity results, even though the CeO_2 samples they prepared had similar morphologies. This may be attributed to the fact that the catalytic activity of CeO_2 for CO oxidation is influenced by many factors. Among them, the amount of surface oxygen species (representation for OSC, Oxygen Storage Capacity) and its reducibility are vital characteristics to determine the properties of CeO_2.

In this paper, CeO_2 in nanoscale with different morphologies of rod, tube and cube were prepared through a hydrothermal process. The catalytic performance of these CeO_2 samples for CO oxidation was investigated. The results exhibited that the rod-like CeO_2 showed a far superior activity to the other two catalysts. The cause is discussed, and the highly reducible oxygen species on the surface of CeO_2 nanorods is considered to be the main reason.

2. Results and Discussion

2.1. Catalyst Characterization

XRD patterns of the three CeO_2 samples with different morphologies are shown in Figure 1. There were diffraction peaks at 2θ = 28.5°, 33.1°, 47.5°, 56.3°, 59.1°, 69.4°, 76.7° and 79.1°, which can be ascribed to the {111}, {200}, {220}, {311}, {222}, {400}, {331} and {420} planes of CeO_2, respectively. The patterns agree well with those of CeO_2 with fluorite structure (JCPDS Card No. 43-1002). There was no significant difference between the patterns of CeO_2-R and CeO_2-C, and the peaks were strong and sharp. However, the peaks in the pattern of CeO_2-T were relatively weak and the full width at half maximum (FWHM) was larger than those of the other two samples. This indicates that CeO_2-T is composed of small crystal particles.

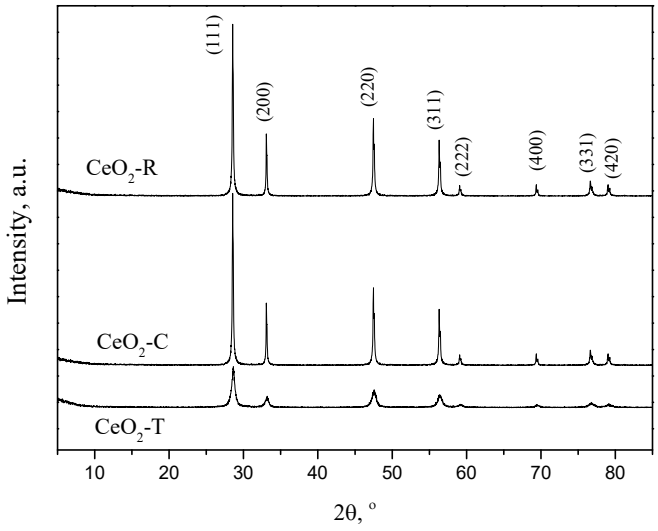

Figure 1. XRD patterns of CeO_2 with different morphologies.

The morphologies of the three CeO_2 samples were characterized by SEM and TEM. As shown in Figure 2a1,a2, CeO_2-R are rod-like particles with lengths of 300 nm–1 μm and diameters of 20–40 nm. Moreover, it can be seen from the SEM image of CeO_2-R, there were some plate-like particles. However, in the TEM image, it is almost impossible to find the particles with the 'two dimensional' structure. Maybe the ultrasonic treatment during the sample preparation for TEM measurement would be the cause for the disappearance of the special structure.

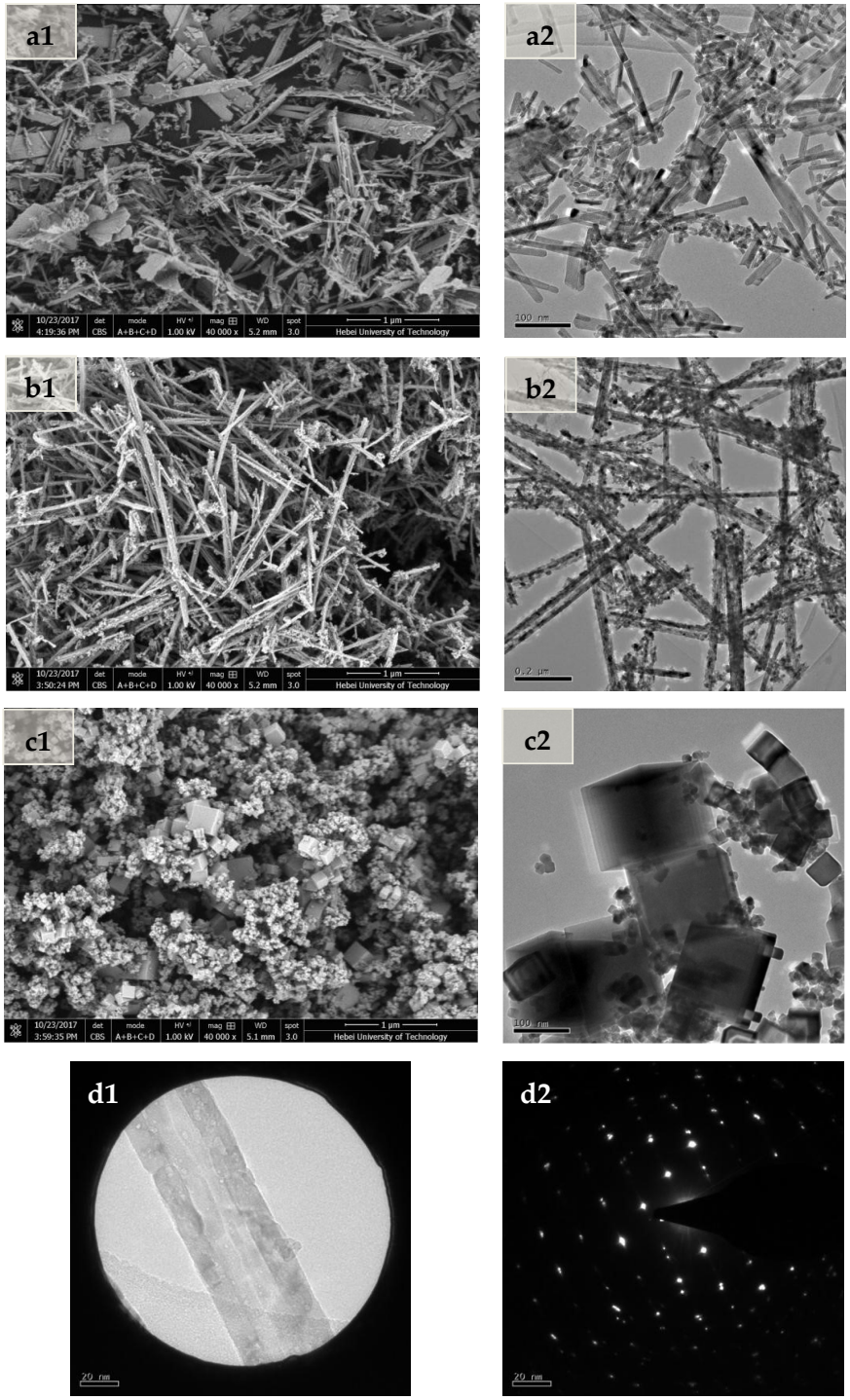

Figure 2. SEM and TEM images of CeO_2 with different morphologies. (**a1**,**b1**,**c1**) are SEM images of CeO_2-R, CeO_2-T and CeO_2-C; (**a2**,**b2**,**c2**) are TEM images of CeO_2-R, CeO_2-T and CeO_2-C; (**d1**,**d2**) are SAED of CeO_2-T.

CeO_2-T particles represent the straight tube morphology with lengths of 1–5 μm and external diameters of 30–70 nm (Figure 2a2,b2). Some near-spherical shape particles, with sizes smaller than 30 nm are also found adhered to the outside of the tube. In addition, from the SEM image, part of the CeO_2-T shows the side-opening tube structure. Zhao et al. [25] indicated that CeO_2 nanotubes might be formed through a process of dissolution-recrystallization, anisotropic growth and self-crimping of the $Ce(OH)_3$ crystal seed. Under the influence of P123, $Ce(OH)_3$ grew along the {110} direction and presented a sheet structure. Then the self-crimping of the sheet structure occurred to reduce the surface energy and it ended with a tube structure. The unfinished self-crimping would lead to a side-opening tube structure. As shown in Figure 2b2, the TEM image of CeO_2-T reveals that its tube wall was composed of small CeO_2 crystals, with diameters less than 20 nm, which are much smaller than those which formed the particles of CeO_2-R or CeO_2-C. This is consistent with the results of XRD. However, some ordered tube-like structures are also found in CeO_2-T (Figure 2d1). The SAED (Selected Area Electron Diffraction) patterns are shown in Figure 2d2, and the bright point reflections indicate the tube-like particles observed were monocrystals.

Figure 2c1 gives the SEM image of CeO_2-C. It can be clearly seen that CeO_2 particles of different sizes with cubic morphology were formed along with many small particles. The TEM image, Figure 2c2, shows that the small particles also had cube like morphologies. The particles of CeO_2-C, with length of the side about 40–280 nm, had smooth surfaces and ordered morphologies.

The textural properties of the three CeO_2 catalysts were investigated by N_2 adsorption- desorption at 196 °C, and the results are shown in Table 1 and Figure 3. The specific surface areas of CeO_2-R (51.4 m^2/g) and CeO_2-T (55.6 m^2/g) were much larger than that of CeO_2-C (9.3 m^2/g), which is due to the secondary pores that formed by the packing of CeO_2 particles with one-dimensional structures, both rod and tube. In addition, the surface area of CeO_2-T was a little larger than that of CeO_2-R, which might be attributed to its tubular structure that has two surfaces of inside and outside. As shown in Figure 3, all of the three samples exhibited type IV adsorption isotherms with hysteresis loops of an H3 type, which were due to capillary condensation in mesoporous pores. It can also be seen in Figure 3 that the pores of all CeO_2 samples were in the mesoporous range, and the pore size distribution of CeO_2-R was more uniform. The adsorption capacity of N_2 on CeO_2-C was very small, which is accordance with its small surface area.

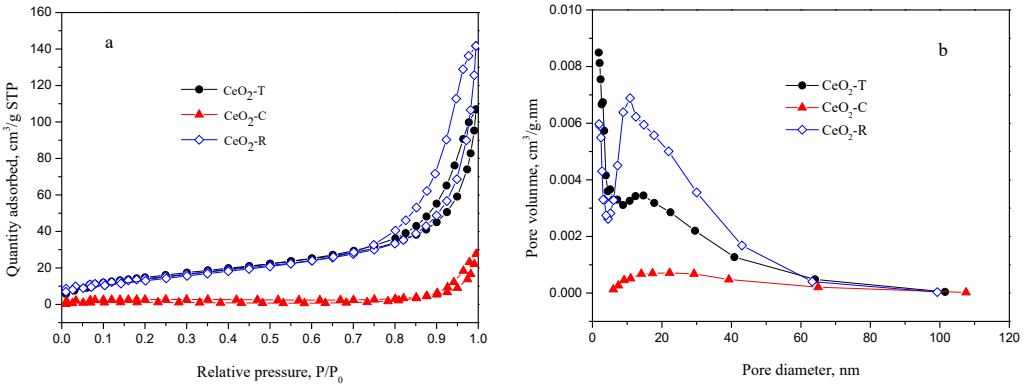

Figure 3. N_2 adsorption-desorption isotherms (**a**) and pore size distribution (**b**) of CeO_2 with different morphologies.

Table 1. Textural properties of CeO_2 samples and their catalytic performance for CO oxidation.

Entry	Catalyst	S_{BET} (m^2/g)	Pore Volume (cm^3/g)	Pore Diameter (nm)	Reaction Temperature (°C) [1]		
					T_{10}	T_{50}	T_{90}
1	CeO_2-R	51.4	0.218	14.2	158	216	228
2	CeO_2-T	55.6	0.158	11.5	203	278	366
3	CeO_2-C	9.3	0.043	29.8	253	325	375

[1] m(Cat) = 500 mg; GHSV = 12,000 mL·$gcat^{-1}$·h^{-1}; T_{10}, T_{50} and T_{90} represent temperatures that CO conversions are 10%, 50% and 90%, respectively.

2.2. CO Oxidation Catalyzed by CeO_2

The three CeO_2 samples with different morphologies were evaluated for their activity in CO oxidation. The results are shown in Figure 4 and Table 1. The CO conversion increased with temperature over all three CeO_2 catalysts and CeO_2-R exhibited the highest activity. Moreover, the catalytic activity of CeO_2-R for CO oxidation was sensitive to reaction temperature. The CO conversion was 28.8% at 200 °C, and it increased promptly to 90.0% at 228 °C. CeO_2-T showed almost the same T_{90} as CeO_2-C, but its activity at low temperature was superior to the latter. Because of the relatively large specific surface area, CeO_2 with tube like morphologies usually exhibits higher activity in catalytic reaction than the others. Pan et al. [26] found that CeO_2 nanotubes gave the best activity for CO oxidation among CeO_2 with various morphologies, and they believed this could be due to its high surface area. Zhao et al. [27] also found CeO_2 nanotubes demonstrated better catalytic activity on methylene blue decolorization, which could be explained by the exposure of higher active surface {110} and considerable defects on the surface of the CeO_2 nanotubes.

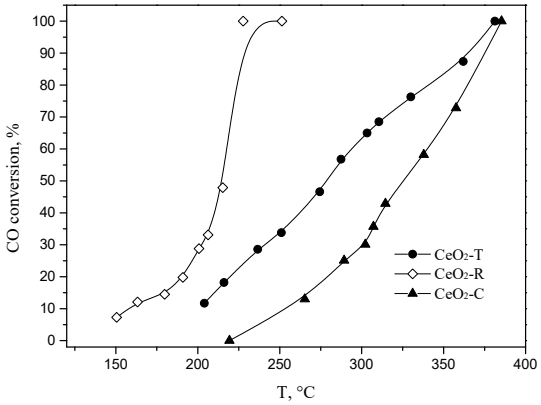

Figure 4. Catalytic activity of CeO_2 with different morphologies in CO oxidation.

To find out the reasons for the difference between the catalytic performance of the three catalysts, H_2-TPR measurements were carried out. The results are exhibited in Figure 5 and Table 2.

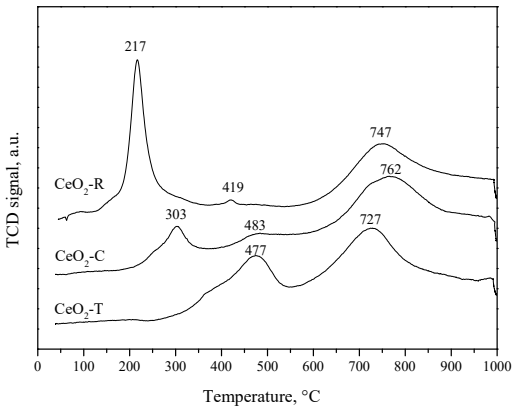

Figure 5. H_2-TPR curves of CeO_2 with different morphologies.

Table 2. H_2-TPR results of CeO_2 with different morphologies.

Sample	Peak Temperature (°C)			H_2 Uptake (μmol/g)		
	Surface O-II	Surface O	Bulk O	Surface O-II	Surface O	Bulk O
CeO_2-T	—	477	727	—	415	697
CeO_2-C	303	483	762	193	208	668
CeO_2-R	217	419	747	436	26	665

There were two reduction peaks at 477 °C and 727 °C in TPR curve of CeO_2-T. The low temperature peak was attributed to the reduction of surface oxygen species. The latter, high temperature peak, was attributed to the lattice oxygen in the bulk phase [18]. Unlike CeO_2-T's, in the TPR curve of CeO_2-C, there was a third peak at 303 °C besides the surface and bulk phase oxygen peak at 483 °C and 762 °C. Table 2 gives the H_2 consumption in relation to the reduction peaks, and it suggests that the bulk oxygen amounts in CeO_2-T and CeO_2-C were almost equal. However, the surface oxygen quantity in CeO_2-C was much lower than that in CeO_2-T. If the H_2 consumption of the peak at 303 °C is counted, the surface oxygen quantity of CeO_2-C (401 μmol/g) approximately equaled that of CeO_2-T (415 μmol/g). Thus, the peak at 303 °C should be attributed to another kind of surface oxygen species that can be reduced at much lower temperature, which could be called Surface O-II. It is usually considered that the surface oxygen of CeO_2 shows higher activity and can easily react with the adsorbed CO [27]. Gurbani et al. [28] indicated that the higher redox capacity of the catalyst, the higher activity for CO oxidation. Therefore, according to the H_2-TPR results, CeO_2-C should have superior activity to CeO_2-T for CO oxidation. However, the evaluation shows the opposite result and CeO_2-T exhibited higher activity than CeO_2-C. This may due to the large surface area of CeO_2-T (55.6 m^2/g) compared to CeO_2-C (9.3 m^2/g). Li et al. [29] prepared CeO_2 samples with different surface areas (67–205 m^2/g) and found that the catalytic activity for CO oxidation increased with a specific surface area of CeO_2. Guo et al. [30] also revealed similar results using CeO_2 catalysts with surface areas of 21–364 m^2/g.

Similar to CeO_2-C, there were three reduction peaks in the TPR curve of CeO_2-R. The bulk oxygen reduction temperature was 747 °C, and the surface oxygen reduction temperature decreased to 419 °C with a small H_2 consumption of 26 μmol/g. The third strongest reduction peak was at 217 °C with a H_2 consumption of 436 μmol/g. All the data above-mentioned reveal that there were a large amount of surface oxygen species which could be reduced easily and were more active for CO oxidation. Moreover, CeO_2-R had a relatively large specific surface area (51.4 m^2/g) which was also one of the causes for its high activity.

In addition, High Resolution Transmission Electron Microscope (HRTEM) was conducted to confirm the shape and size of CeO_2-R and CeO_2-T particles. Figure 6a shows that the surface of CeO_2-R was smooth and its growth direction was along the {110} orientation. While CeO_2-T (Figure 6b) was composed of small particles, smaller than 20 nm, which assembled the hollow tubular structure. Zhou et al. [31] has indicated that CeO_2 nanorods had unusually exposed {001} and {110} planes which were more reactive for CO oxidation than the irregular nanoparticles, that exposed more of the stable {111} planes. Therefore, in this study, the catalytic activity of CeO_2-T for CO oxidation was inferior to that of CeO_2-R, because the former was a combination of small particles and did not have the characteristics of CeO_2 nanotubes, though it had a tubular-like structure.

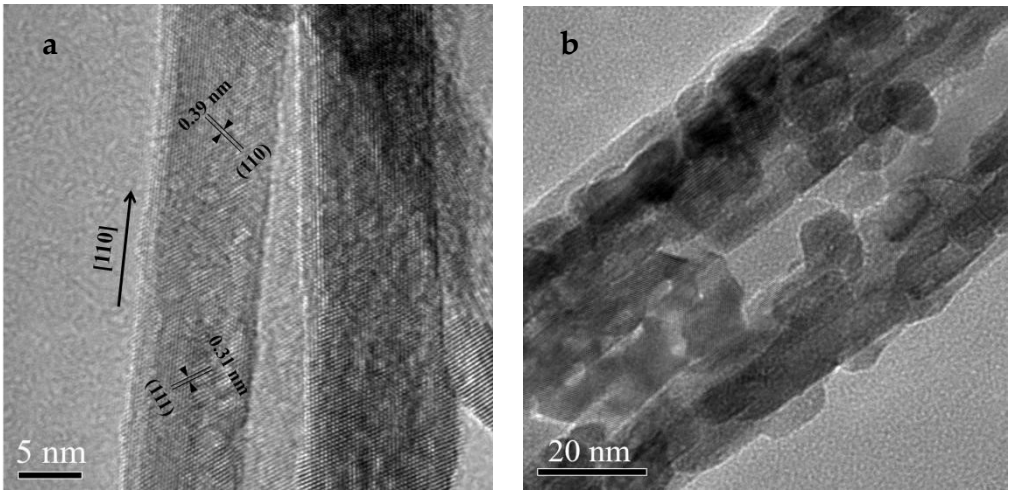

Figure 6. HRTEM images of CeO_2-R (**a**) and CeO_2-T (**b**).

A comparison of the activity of CeO_2-R with reported catalysts is illustrated in Table 3. Because the feed gas composition and space velocity were different, the values here allow only a qualitative comparison. It can be seen from the data in Table 3 that CeO_2-R provided the lowest T_{90} which means the best catalytic activity. However, it's worth noting that CeO_2 core-shell microspheres, reported by Zhang et al. [32], also exhibited excellent activity for CO oxidation with T_{90} of 275 °C when space velocity was 60,000 mL·gcat^{-1}·h^{-1}, though the reduction temperature of surface oxygen species over their catalyst was much higher than that of CeO_2-R. Combined with our experimental results and data from references, it could be concluded that it's not easy to determine the catalytic activities of CeO_2 samples for CO oxidation. Many factors, including morphology, size, texture properties, oxygen species reducibility, and/or something else, may influence the reaction synergistically.

Table 3. Comparison of different CeO_2 catalysts for CO oxidation.

Catalyst	S_{BET} (m^2/g)	T_{SOR} [1] (°C)	Feed Gas (mL·gcat^{-1}·h^{-1})	T_{90} (°C)	References
CeO_2-R	51.4	217	CO:O_2:N_2 = 1%/9%/90% (12,000)	228	This work
CeO_2-R	51.4	217	CO:O_2:N_2 = 1%/9%/90% (18,000)	242	This work
CeO_2-R	51.4	217	CO:O_2:N_2 = 1%/9%/90% (24,000)	253	This work
cauliflower like CeO_2	74.5	490	CO:O_2:He = 1%/20%/79% (60,000)	370 [2]	[24]
CeO_2 nanowires	130	~527 [3]	CO:O_2:He = 1%/21%/78% (9000)	300	[22]
CeO_2 nanorods	128	~520 [3]	CO:O_2:He = 1%/21%/78% (9000)	310	[22]
CeO_2 nanoparticles	364	—	CO:O_2:N_2 = 1%/1%/98% (4800)	282	[30]
CeO_2 core-shell microspheres	87.8	487	CO:O_2:N_2 = 1%/20%/79% (60,000)	275	[32]

[1] Surface oxygen species reduction temperature. [2] The temperature for 98% CO conversion. [3] The temperature was obtained from the TPR curve directly because the authors did not give the exact data.

3. Materials and Methods

3.1. Materials

All of the reagents were analytical grade and used without further purification. Polyethylene oxide-polypropylene oxide-polyethyleneoxide (PEO-PPO-PEO) triblock co-polymers (P123) was purchased from Sigma-Aldrich (ST. Louis, MO, USA). Cerium (III) chloride heptahydrate, cerium (III) nitrate nexahydrate, aqueous ammonia (25%) and sodium hydroxide were purchased from Sinoreagent (Shanghai, China).

3.2. Preparation of CeO_2 with Different Morphologies

3.2.1. CeO_2 Nanorods

Preparation of CeO_2 nanorods was carried out via a hydrothermal process. Typically, 6 g of $Ce(NO_3)_3$·$6H_2O$, 84 g of NaOH and 150 mL of deionized water were mixed and stirred for 30 min. Then, the mixture was transferred into an autoclave with a Teflon liner and underwent the hydrothermal reaction process at 110 °C for 24 h. After that, the precipitate was filtered, repeatedly washed with deionized water (Jingchun, Tianjin, China) and anhydrous ethanol (Kermel, Tianjin, China) several times until the pH reached 7. Finally, it was dried at 80 °C and calcined at 500 °C for 4 h. The obtained sample was rod-like CeO_2 and denoted as CeO_2-R.

3.2.2. CeO_2 Nanotubes

Firstly, 17.4 g of P123 with a molecule of 5800 was dissolved in a mixture of 60 mL ethanol and 60 mL deionized water in an ultrasonic water bath for 1 h at room temperature. Then, 5.58 g of $CeCl_3$·$7H_2O$ was added into the solution and stirred for 30 min. After that, NH_3·H_2O was added dropwise until the pH was adjusted to 10 and a red flocculent precipitate was formed. After stirring for another 1 h, the mixture was transferred into an autoclave with a Teflon liner for the hydrothermal reaction process at 160 °C for 72 h. Thirdly, the precipitate was filtered, repeatedly washed with

deionized water and anhydrous ethanol several times until the pH reached 7. Finally, the solid was dried at 80 °C and calcined at 500 °C for 4 h. The obtained sample was denoted as CeO_2-T.

3.2.3. CeO_2 Nanocubes

Typically, 6 g of $Ce(NO_3)_3 \cdot 6H_2O$, 84 g of NaOH and 150 mL of deionized water were mixed and stirred for 30 min. Then, the mixture was transferred into an autoclave with a Teflon liner and underwent the hydrothermal reaction process at 160 °C for 24 h. After that, the precipitate was filtered, repeatedly washed with deionized water and anhydrous ethanol several times until the pH reached 7. Finally, it was dried at 80 °C and calcined at 500 °C for 4 h. The sample was denoted as CeO_2-C.

3.3. Catalyst Characterization

X-ray diffraction (XRD) patterns were recorded using a Rigaku D/Max-2500 X-ray diffractometer (Tokyo, Japan) with Cu Kαradiation (40 kV, 100 mA) at the scanning range of 5°–85°. The scanning electron microscopy (SEM) images were recorded on a FEI Nova NanoSEM 450 (Hillsboro, OR, USA) and all samples were gold-coated. Transmission electron microscope (TEM) images and selected area electron diffraction (SAED) were obtained with a FEI Tecnai G2 F20 (Hillsboro, OR, USA) at 200 kV.

The textural properties of the samples were measured by a N_2 adsorption–desorption method using a Micromeritics ASAP 2020 M+C physisorption analyzer (Norcross, GA, USA). The specific surface area was calculated by a BET method. Hydrogen temperature-programmed reduction (H_2-TPR) was carried out using a Micromeritics AutoChem II-2920 automated catalyst characterization system (Norcross, GA, USA). The sample (0.1 g) was purged in Ar (50 mL/min) at ambient temperature. After that, the flowing gas was changed to a H_2/Ar mixture (10%/90%, 50 mL/min) and the sample was heated to 1000 °C at an increasing rate of 10 °C/min. The H_2 consumption was tested using a thermal conductivity detector (TCD).

3.4. Catalytic Activity Tests

The catalytic activity test for CO oxidation was performed in a fixed-bed reactor (a stainless steel tube reactor with an inner diameter of 10 mm and length of 30 cm) at atmospheric pressure in the temperature range of 150–400 °C. The catalyst (500 mg, 40–60 mesh) was mounted in the reactor, and the reaction gas mixture ($CO:O_2:N_2$ = 1%:9%:90%) was fed through the catalyst bed at a designed flow rate.

The composition of the gas mixture was analyzed using an online Agilent 7890B gas chromatograph (Agilent Technologies, Santa Clara, CA, USA) equipped with a TCD detector. The CO conversion (X_{CO}) was calculated as follows:

$$X_{CO}(\%) = \frac{[CO]_{in} - [CO]_{out}}{[CO]_{in}} \times 100$$

4. Conclusions

In summary, nanostructured CeO_2 samples with rod (CeO_2-R), cubic (CeO_2-C) and tube (CeO_2-T) morphologies were prepared through a hydrothermal method. It was shown that CeO_2-R exhibits the highest catalytic activity for CO oxidation (T_{90} was 228 °C at space velocity of 12,000 mL·gcat^{-1}·h^{-1}) than the prepared samples with other morphologies, such as CeO_2-T and CeO_2-C. Characterization of the CeO_2-R catalyst has shown that there are much more easily reducible oxygen species, with a reduction temperature of 217 °C on its surface, which was responsible for the high catalytic activity. It should be emphasized that CeO_2-R sample possessed a large specific surface area (51.4 m^2/g), that could be another reason of its superior activity.

Author Contributions: Investigation, G.F. and W.H.; writing and original draft preparation, G.F. and Z.W.; writing, review and editing, F.L. and W.X.; project administration, W.X.

Funding: This research was funded by Natural Science Foundation of Hebei [B2015202228], Natural Science Foundation of Tianjin [17JCYBJC20100] and the Funding Programme for Scientific Activities of Selected Returns from abroad of Hebei [CL201605].

Conflicts of Interest: The authors declare no conflicts of interest.

References

1. Wang, J.X.; Zhuo, Y.; Zhou, Y.; Wang, H.J.; Yuan, R. Ceria doped zinc oxide nanoflowers enhanced luminol-based electrochemiluminescence immunosensor for amyloid-β detection. *ACS Appl. Mater. Interfaces* **2016**, *8*, 12968–12975. [CrossRef] [PubMed]
2. Suzuki, K.; Miyazaki, H.; Yuzuriha, Y.; Maru, Y.; Izu, N. Characterization of a novel gas sensor using sintered ceria nanoparticles for hydrogen detection in vacuum conditions. *Sens. Actuators B. Chem.* **2017**, *250*, 617–622. [CrossRef]
3. Chandrakala, E.; Praveen, J.P.; Kumar, A.; James, A.R.; Das, D. Strain-induced structural phase transition and its effect on piezoelectric properties of (BZT-BCT)-(CeO_2) ceramics. *J. Am. Ceram. Soc.* **2016**, *99*, 3659–3669. [CrossRef]
4. Kim, C.K.; Kim, T.; Choi, I.Y.; Soh, M.; Kim, D.; Kim, Y.J.; Jang, H.; Yang, H.S.; Kim, J.Y.; Park, H.K.; et al. Ceria nanoparticles that can protect against ischemic stroke. *Angew. Chem. Int. Ed.* **2012**, *51*, 11039–11043. [CrossRef] [PubMed]
5. Xu, C.; Lin, Y.; Wang, J.; Wu, L.; Wei, W.; Ren, J.; Qu, X. Nanoceria-triggered synergetic drug release based on CeO_2-capped mesoporous silica host-guest interactions and switchable enzymatic activity and cellular effects of CeO_2. *Adv. Healthc. Mater.* **2013**, *2*, 1591–1599. [CrossRef] [PubMed]
6. Montini, T.; Melchionna, M.; Monai, M.; Fornasiero, P. Fundamentals and catalytic applications of CeO_2-based materials. *Chem. Rev.* **2016**, *116*, 5987–6041. [CrossRef] [PubMed]
7. Mei, Z.; Li, Y.; Fan, M.; Zhao, L.; Zhao, J. Effect of the interactions between Pt species and ceria on Pt/ceria catalysts for water gas shift: The XPS studies. *Chem. Eng. J.* **2015**, *259*, 293–302. [CrossRef]
8. Manwar, N.R.; Chilkalwar, A.A.; Nanda, K.K.; Chaudhary, Y.S.; Subrt, J.; Rayalu, S.S.; Labhsetwar, N.K. Ceria supported Pt/PtO-nanostructures: Efficient photocatalyst for sacrificial donor assisted hydrogen generation under visible-NIR light irradiation. *ACS Sustain. Chem. Eng.* **2016**, *4*, 2323–2332. [CrossRef]
9. Haneda, M.; Kaneko, T.; Kamiuchi, N.; Ozawa, M. Improved three-way catalytic activity of bimetallic Ir–Rh catalysts supported on CeO_2–ZrO_2. *Catal. Sci. Technol.* **2015**, *5*, 1792–1800. [CrossRef]
10. Alikin, E.A.; Vedyagin, A.A. High temperature interaction of rhodium with oxygen storage component in three-way catalysts. *Top. Catal.* **2016**, *59*, 1033–1038. [CrossRef]
11. Lykhach, Y.; Figueroba, A.; Camellone, M.F.; Neitzel, A.; Skála, T.; Negreiros, F.R.; Vorokhta, M.; Tsud, N.; Prince, K.C.; Fabris, S.; et al. Reactivity of atomically dispersed Pt^{2+} species towards H_2: Model Pt-CeO_2 fuel cell catalyst. *Phys. Chem. Chem. Phys.* **2016**, *18*, 7672–7679. [CrossRef] [PubMed]
12. Ang, M.L.; Oemar, U.; Saw, E.T.; Mo, L.; Kathiraser, Y.; Chia, B.H.; Kawi, S. Highly active Ni/xNa/CeO_2 catalyst for the water–gas shift reaction: Effect of sodium on methane suppression. *ACS Catal.* **2014**, *4*, 3237–3248. [CrossRef]
13. Mamontov, G.V.; Grabchenko, M.V.; Sobolev, V.I.; Zaikovskii, V.I.; Vodyankina, O.V. Ethanol dehydrogenation over Ag-CeO_2/SiO_2 catalyst: Role of Ag-CeO_2 interface. *Appl. Catal. A–Gen.* **2016**, *528*, 161–167. [CrossRef]
14. Wang, C.; Wen, C.; Lauterbach, J.; Sasmaz, E. Superior oxygen transfer ability of Pd/MnOx-CeO_2 for enhanced low temperature CO oxidation activity. *Appl. Catal. B. Environ.* **2017**, *206*, 1–8. [CrossRef]
15. Hou, T.; Yu, B.; Zhang, S.; Xu, T.; Wang, D.; Cai, W. Hydrogen production from ethanol steam reforming over Rh/CeO_2 catalyst. *Catal. Commun.* **2015**, *58*, 137–140. [CrossRef]
16. Wang, Y.; Zhao, J.; Wang, T.; Li, Y.; Li, X.; Yin, J.; Wang, C. CO_2 photoreduction with H_2O vapor on highly dispersed CeO_2/TiO_2 catalysts: Surface species and their reactivity. *J. Catal.* **2016**, *337*, 293–302. [CrossRef]
17. Li, Y.; Shen, W. Morphology-dependent nanocatalysis on metal oxides. *Sci. China Chem.* **2012**, *55*, 2485–2496. [CrossRef]
18. Yuan, Y.; Wang, Z.; An, H.; Xue, W.; Wang, Y. Oxidative carbonylation of phenol with a Pd-O/CeO_2-nanotube catalyst. *Chin. J. Catal.* **2015**, *36*, 1142–1154. [CrossRef]

19. Gawade, P.; Mirkelamoglu, B.; Ozkan, U.S. The role of support morphology and impregnation medium on the water gas shift activity of ceria-supported copper catalysts. *J. Phys. Chem. C* **2010**, *114*, 18173–18181. [CrossRef]
20. Hou, F.; Li, H.; Yang, Y.; Dong, H.; Cui, L.; Zhang, X. Preparation and catalytic oxidation of CO with specific morphology and porous nano CeO_2. *Chem. Ind. Eng. Prog.* **2017**, *36*, 2481–2487. [CrossRef]
21. Zhou, Y.; Wang, Z.; Liu, C. Perspective on CO oxidation over Pd-based catalysts. *Catal. Sci. Technol.* **2015**, *5*, 69–81. [CrossRef]
22. Ta, N.; Zhang, M.; Li, J.; Li, H.; Li, Y.; Shen, W. Morphology-dependent redox and catalytic properties of CeO_2 nanostructures: Nanowires, nanorods and nanoparticles. *Catal. Today* **2009**, *148*, 179–183. [CrossRef]
23. González-Rovira, L.; Sánchez-Amaya, J.M.; López-Haro, M.; del Rio, E.; Hungría, A.B.; Midgley, P.; Calvino, J.J.; Bernal, S.; Botana, F.J. Single-step process to prepare CeO_2 nanotubes with improved catalytic activity. *Nano Lett.* **2009**, *9*, 1395–1400. [CrossRef] [PubMed]
24. Zhang, X.; Hou, F.; Yang, Y.; Wang, Y.; Liu, N.; Chen, D.; Yang, Y. A facile synthesis for cauliflower like CeO_2 catalysts from Ce-BTC precursor and their catalytic performance for CO oxidation. *Appl. Surf. Sci.* **2017**, *423*, 771–779. [CrossRef]
25. Zhao, X.B.; You, J.; Lu, X.W.; Chen, Z.G. Hydrothermal synthesis, characterization and property of CeO_2 nanotube. *J. Inorg. Mater.* **2011**, *26*, 159–164. [CrossRef]
26. Pan, C.; Zhang, D.; Shi, L.; Fang, J. Template-free synthesis, controlled conversion, and CO oxidation properties of CeO_2 nanorods, nanotubes, nanowires, and nanocubes. *Eur. J. Inorg. Chem.* **2008**, *15*, 2429–2436. [CrossRef]
27. Zhan, W.C.; Guo, Y.; Gong, X.Q.; Guo, Y.L.; Wang, Y.Q. Surface oxygen activation on CeO_2 and its catalytic performances for oxidation reactions. *Sci. Sin. Chim.* **2012**, *42*, 433–445. [CrossRef]
28. Gurbani, A.; Ayastuy, J.L.; González-Marcos, M.P.; Gutiérrez-Ortiz, M.A. CuO-CeO_2 catalysts synthesized by various methods: Comparative study of redox properties. *Int. J. Hydrogen Energy* **2010**, *35*, 11582–11590. [CrossRef]
29. Li, X.; Chen, F.; Lu, X.; Ni, C.; Chen, Z. Modified-EISA synthesis of mesoporous high surface area CeO_2 and catalytic property for CO oxidation. *J. Rare Earth* **2009**, *27*, 943–947. [CrossRef]
30. Guo, M.N.; Guo, C.X.; Jin, L.Y.; Wang, Y.J.; Lu, J.Q.; Luo, M.F. Nano-sized CeO_2 with extra-high surface area and its activity for CO oxidation. *Mater. Lett.* **2010**, *64*, 1638–1640. [CrossRef]
31. Zhou, K.; Wang, X.; Sun, X.; Peng, Q.; Li, Y. Enhanced catalytic activity of ceria nanorods from well-defined reactive crystal planes. *J. Catal.* **2005**, *229*, 206–212. [CrossRef]
32. Zhang, L.; Zhang, L.; Xu, G.; Zhang, C.; Li, X.; Sun, Z.; Jia, D. Low-temperature CO oxidation over CeO_2 and CeO_2@Co_3O_4 core-shell microspheres. *New J. Chem.* **2017**, *41*, 13418–13424. [CrossRef]